A new three-band, two beam astronomical photo-polarimeter

G. Srinivasulu[1*], A. V. Raveendran[2], S. Muneer[1†], M. V. Mekkaden[3],
N. Jayavel[4], M. R. Somashekar[1], K. Sagayanathan[1], S. Ramamoorthy[1],
M. J. Rosario[5] and K. Jayakumar[6‡]

[1]*Indian Institute of Astrophysics, Bangalore 560034, India*

[2]*399, "Shravanam", 2nd Block, 9th Phase, J P Nagar, Bangalore 560108, India*

[3]*No 82, 17E Main, 6th Block, Koramangala, Bangalore 560095, India*

[4]*No 22, Bandappa lane, New Byappanahalli, Bangalore 560038, India*

[5]*210, 4th Main, Lakshmi Nagar Extn, Porur, Chennai 600116, India*

[6]*24, Postal Nagar, Ampuram, Vellore-632009, India*

Abstract. We designed and built a new astronomical photo-polarimeter that can measure linear polarization simultaneously in three spectral bands. It has a Calcite beam-displacement prism as the analyzer. The ordinary and extra-ordinary emerging beams in each spectral bands are quasi-simultaneously detected by the same photomultiplier by using a high speed rotating chopper. A rotating superachromatic Pancharatnam halfwave plate is used to modulate the light incident on the analyzer. The spectral bands are isolated using appropriate dichroic and glass filters.

We show that the reduction of 50% in the efficiency of the polarimeter because of the fact that the intensities of the two beams are measured alternately is partly compensated by the reduced time to be spent on the observation of the sky background. The use of a beam-displacement prism as the analyzer completely removes the polarization of background skylight, which is a major source of error during moonlit nights, especially, in the case of faint stars.

The field trials that were carried out by observing several polarized and unpolarized stars show the performance of the polarimeter to be satisfactory.

Keywords : instrumentation: polarimeters – techniques: polarimetric – methods: observational, data analysis

*email: gs@iiap.res.in

†email: muneers@iiap.res.in

‡email: jayakumar.kanniah@gmail.com

1.   Introduction

There was a need for an efficient photo-polarimeter for observations with the 1-m Carl Zeiss Telescope at Vainu Bappu Observatory, Kavalur. The single spectral band, star–sky chopping polarimeter, which was built by Jain & Srinivasulu (1991) almost a quarter century ago, was the only available instrument for polarimetric studies (Ashok et al. 1999; Parthasarathy, Jain & Bhatt 2000; Manoj, Maheswar & Bhatt 2002; Raveendran 1999, 2002). The star-sky chopping procedure makes the instrument very inefficient, thereby underutilizing the available telescope time.

A project to build a new photo-polarimeter for observations of point sources was initiated in the Indian Institute of Astrophysics quite sometime back. Unfortunately, due to unforeseen reasons there were delays at various stages of the execution of the project. There were several ongoing programmes in the Institute which required accurate multiband polarimetry: studies of Herbig Ae/Be stars (Ashok et al. 1999), Luminous Blue variables (Parthasarathy et al. 2000), Young Stellar Objects (Manoj et al. 2002), R CrB stars (Kameswara Rao & Raveendran 1993), RV Tauri stars (Raveendran 1999), Mira variables that show long-term modulations in their brightness at light maximum (Raveendran 2002) and T Tauri stars (Mekkaden 1999).

The new polarimeter, which was designed and built in the Institute, was mounted onto the 1-m telescope and observations of several polarized and unpolarized stars were made during April–May 2014, to determine its suitability for efficient astronomical observations. Due to prevalent poor sky conditions, the instrument could be used effectively only on a few nights during this period. The instrument was found to have a very high mechanical stability, but a comparatively low polarization efficiency of 94.72%. Since we suspected the scattered light inside the instrument to be the reason for such a low value for the efficiency, we blackened the few internal mechanical parts which were left out earlier, and again made observations during February–April 2015.

In this paper we discuss the details that have gone in the selection of the analyzer and give brief descriptions of the component layout, the control electronics, and the data acquisition procedure and analysis. Details of the polarimeter and the data reduction procedure can be found in Raveendran et al. (2015). We also discuss the results of the observation made during February–April 2015, which were carried out to evaluate the performance of the instrument.

2.   Choice of the analyzer

In order to reduce the adverse effects of the atmospheric scintillation, seeing and transparency variation, which usually limit the accuracy of any polarimetric measurement, it is imperative to measure simultaneously both the emerging beams, ordinary and extra-ordinary, from the analyzer. The two basically different types of analyzers that are usually employed in astronomical polarimeters are: (1) beam-displacement prisms made of Calcite (Piirola 1973; Magalhaes & Velloso 1988; Scaltriti et al. 1989; Schwarz & Piirola 1999) and (2) beam-splitting prisms of Wol-
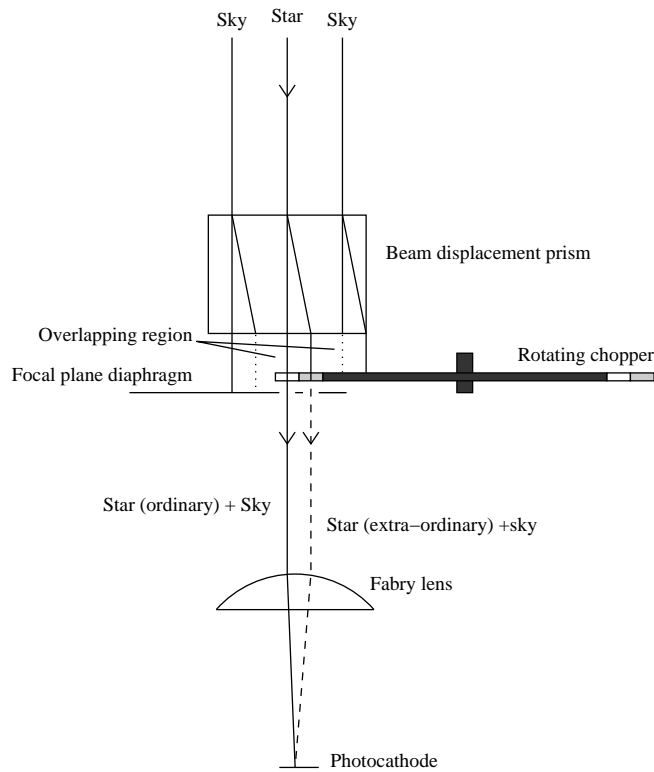
Sky   Star   Sky

Beam displacement prism

Overlapping region

Focal plane diaphragm

Rotating chopper

Star (ordinary) + Sky

Star (extra–ordinary) +sky

Fabry lens

Photocathode

Figure 1. Working principle of the polarimeter.

laston or Foster design (Magalhaes, Benedetti & Roland 1984; Deshpande et al. 1985; Kikuchi 1988; Hough, Peacock & Bailey 1991)

We adopted a design for the polarimeter incorporating a Calcite beam-displacement prism so that most of the spectroscopic nights that are available at the site can be utilized for polarimetric observations. The working principle of the polarimeter is illustrated in Fig. 1. An astronomical polarimeter based on this principle was first built by Piirola (1973). A beam-displacement prism divides the incident light, producing two spatially separated emerging beams with mutually perpendicular planes of polarization. The background sky, which acts as an extended object, illuminates the entire top surface of the beam-displacement prism, and hence, produces two broad emergent beams whose centres are spatially separated. There will be considerable overlap between these two beams about the geometrical axis of the prism, and wherever the beams overlap in the focal plane of the telescope that portion remains unpolarized by the prism and gives the background sky brightness directly. The situation is different with respect to the starlight; the star being a point source, there will be no overlap between the two emergent beams from the prism. The net result of these two effects is that we observe two images of the star with mutually perpendicular planes of polarization at the focal plane, which are superposed on the unpolarized

background sky. Two identical apertures are used to isolate these images, and a rotating chopper is used to alternately block one of the images allowing the other to be detected by the same photomultiplier tube.

The main advantages of such an arrangement are: (i) The contribution of background sky polarization is completely eliminated from the data, thereby, facilitating the observations of fainter stars during moonlit nights without compromising on the accuracy that is achievable during dark nights. This is possible because the background sky is not modulated, it just appears as a constant term that can be removed from the data accurately. (ii) Since the same photomultiplier tube is used to detect both the beams quasi-simultaneously, the effect of any time-dependent variations in its sensitivity as a result of undesired variations in the operating conditions of the associated electronics, like, variations in HT supply, is negligible. (iii) The quasi-simultaneous detection of both the beams using a fast rotating chopper essentially eliminates the adverse effects of the variations in sky-transparency and significantly reduces the errors due to atmospheric scintillation for bright stars. Scintillation noise is independent of the brightness of the star and dominates the photon noise for bright objects; with a 1-m telescope the low frequency (< 50 Hz) scintillation noise is expected to be larger than the photon noise for stars brighter than B = 7.0 mag at an airmass of 1.0 (Young 1967). The averaging of the data by the process of long integration will reduce the scintillation noise only to a certain extent because of its log-normal distribution. The frequency spectrum of scintillation noise is flat up to about 50 Hz; the noise amplitude decreases rapidly above this frequency and it becomes negligibly small above 250 Hz. With the fast chopping of the two emergent beams alternately and the automatic removal of the background sky polarization, it is possible to make polarization measurements that are essentially photon-noise limited.

The two factors that determine the overall efficiency of a polarimeter attached to a telescope are (Serkowski 1974a): (i) the faintest magnitude that could be reached with a specified accuracy in a given time, and (ii) the maximum amount of information on wavelength dependence that could be obtained during the same time. It is evident that the former depends on the efficiency in the utilization of photons collected by the telescope and the latter on the number of spectral bands that are simultaneously available for observation. In the beam-displacement prism-based polarimeters, where the image separation is small, the intensities of the two beams produced by the analyzer are measured alternately using the same detector, and hence, only 50 per cent of the light collected by the telescope is effectively utilized. In polarimeters using Wollaston prism as the analyzer, the two beams, which are well-separated without any overlap, can be detected simultaneously by two independent photomultiplier tubes, fully utilizing the light collected (Magalhaes et al. 1984; Deshpande et al. 1985). For simultaneous multi-spectral band observations that make use of the incident light fully, the beams emerging from the analyzer will have to be well-separated so as to accommodate a large number of photomultiplier tubes, making the resulting instrument both heavy and large in size (Serkowski, Mathewson & Ford 1975), and hence, not suitable for the 1-m telescope. Usually, in Wollaston and Foster prism-based polarimeters, which have the provisions for simultaneous observations in multi-spectral bands, different spectral bands are distributed among the two emergent beams, and hence, at a time only 50 per cent of the light collected in each spectral region is made use of (Kikuchi 1988; Hough et al. 1991).

The background sky polarization has to be determined accurately and removed from the object *plus* sky data when there is no overlap between the emergent beams, and a significant fraction of the time spent on object integration will have to be spent for such observations if the objects are faint. In beam-displacement prism-based polarimeters, time has to be spent only to determine the brightness of the background sky, and for the maximum signal-to-noise ratio, it is only a negligible fraction of the object integration time even for relatively faint objects; the available time for observation can be almost entirely utilized to observe the object, as indicated by the analysis presented in section 5.3 on optimum sky background observation. Therefore, the non-utilization of 50 per cent light in beam-displacement prism-based polarimeters does not effectively reduce their efficiency much, especially, while observing faint objects where the photons lost actually matter. The provisions for multi-spectral band observations can be easily incorporated in the design, making beam-displacement prism-based polarimeters to have an overall efficiency significantly higher than that of the usual Wollaston or Foster prism based polarimeters. Another advantage of these polarimeters is that they can be easily converted into conventional photometers, just by pulling the beam-displacement prism out of the light path.

3. Layout of the components

The layout of the polarimeter indicating the positions of the main components is shown schematically in Fig. 2. A super-achromatic halfwave plate of Pancharatnam design is used to rotate the plane of polarization of the incoming light falling on the analyzer, and thereby, to modulate the intensities of the two emergent beams from the analyzer (Frecker & Serkowski 1976). The position angle of the effective optical axis of a Pancharatnam retarder is wavelength-dependent. This would cause difficulties in the accurate determination of the position angle of polarization when broad spectral bands, as in the present case, are used for observations because corrections that are to be applied to the observed position angles would depend on the energy distribution of the observed objects. Such an inconvenience is usually avoided by introducing another stationary identical Pancharatnam plate immediately after the rotating plate in the light path. The introduction of such a half-wave plate ensures that the signal modulation is only a function of the relative positions of the effective optical axes of the two half-wave plates, which is wavelength-independent. The rotating halfwave plate, which acts as the modulator of the incoming light, is the first element in the optical path of the polarimeter, and hence, avoids the detection of any spurious polarization produced by any optical components used in the polarimeter. The two identical half-wave plates of 19 mm clear aperture used in the polarimeter are acquired from Bernhard Halle Nachfl. GmbH, Berlin, Germany.

The analyzer is a cross-mounted, double calcite block with a 20 mm clear aperture and a total thickness of 28 mm, which produces identical ordinary and extraordinary images at the focal plane of the telescope. This component is also acquired from Bernhard Halle Nachfl. GmbH. Since the separation between the emergent beams is a function of wavelength, the images will be slightly dispersed. The image strips have a linear size of 0.318 mm in the spectral interval 320–990 nm with the centre-to-centre distance of the two images being 2.292 mm. The images can be isolated for observation using one of the two sets of twin identical diaphragms of 20 and 25 arc
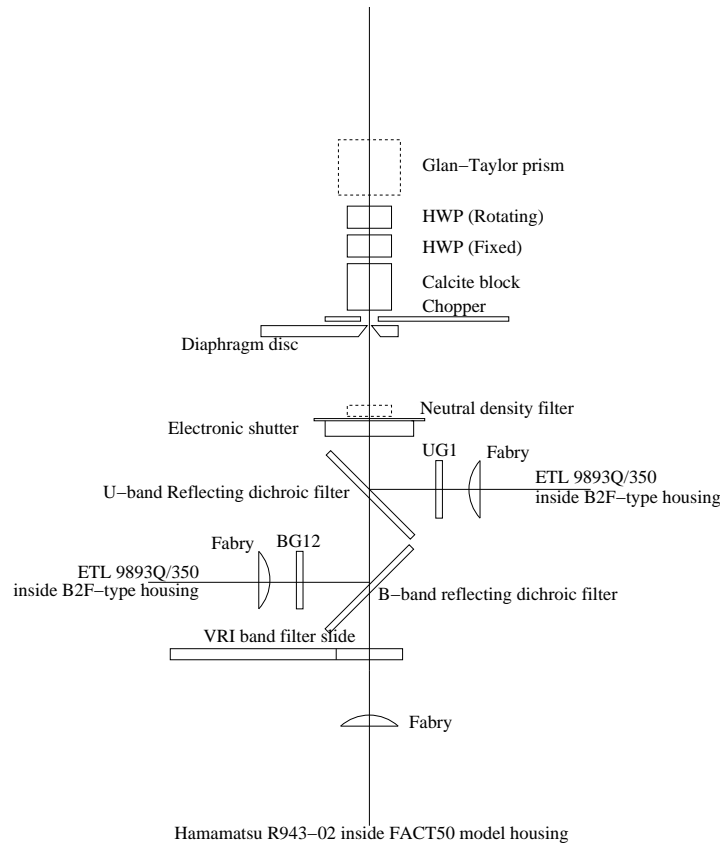
Glan–Taylor prism

HWP (Rotating)
HWP (Fixed)
Calcite block
Chopper

Diaphragm disc

Neutral density filter
Electronic shutter

UG1   Fabry

U–band Reflecting dichroic filter

ETL 9893Q/350
inside B2F–type housing

Fabry   BG12

ETL 9893Q/350
inside B2F–type housing

B–band reflecting dichroic filter

VRI band filter slide

Fabry

Hamamatsu R943–02 inside FACT50 model housing

Figure 2. Schematic layout of the main components of the polarimeter. In the instrument the *U* and *B* bands are mutually perpendicular, making it more compact.

sec in diameter mounted on a manually rotatable disc. The calcite block is placed in the light path immediately after the stationary half-wave plate. The rotating chopper isolates alternately the ordinary or extra-ordinary image for detection by the same photomultiplier. The chopper has four slots, two for each of the images, and therefore the effective chopping frequency is double the rotational frequency of the chopper.

The isolation of the spectral regions into the three bands for simultaneous observation is achieved by using two dichroic filters, one to reflect the ultra-violet part of the incoming light and the other to reflect the blue part of the spectrum from the light transmitted by the first. The dichroic filters used are obtained from Custom Scientific, Inc., Arizona, USA. The reflective coatings required for the dichroism are done on 2 mm thick glass substrates. The two reflected beams are detected by two separate uncooled photomultiplier tubes. The bi-alkali photocathodes of these tubes along with the Schott glass filters inserted in front of them produce spectral bands that approximate the *U* and *B* bands of Johnson. The light transmitted by both the dichroic filters,
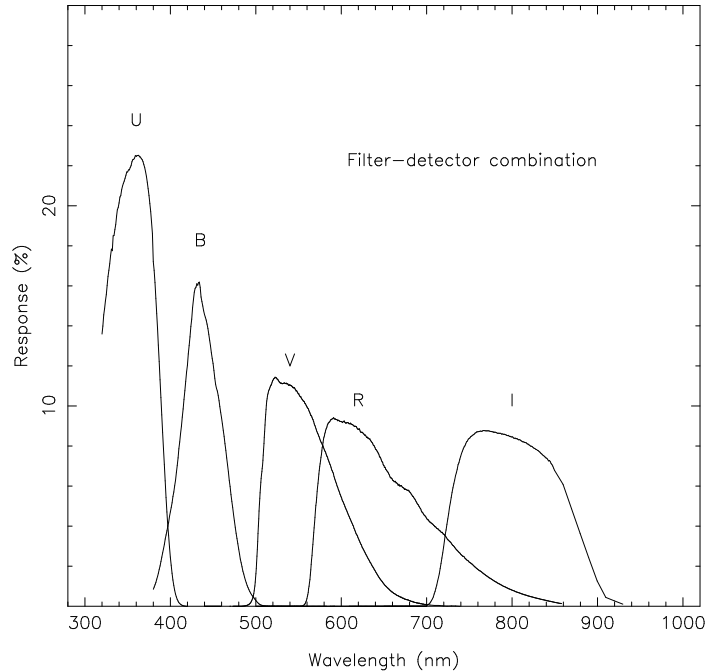
Figure 3. Combined response of the filter-detector combination.

Table 1. Filter-detector combinations.

| Spectral | | Mean wavelength | |
Band	Filter combination	λ_0 (nm)	Photomultiplier tube
U	UG1 (1 mm)	357	ETL 9893Q/350B
B	BG12 (1 mm)	437	ETL 9893Q/350B
V	BG18 (1 mm) + GG495 (2 mm)	561	Hamamatsu R943-02
R	OG570 (2 mm) + KG3 (2 mm)	652	"
I	RG9 (3 mm)	801	"

which fall in the *VRI* spectral bands, is detected by a cooled photomultiplier tube with a GaAs photocathode. The observations are made sequentially in *V*, *R* and *I* bands using suitable filter combinations mounted on a sliding filter-holder. The Schott glass filters that are used have clear apertures of 25 mm diameter. The combined responses of the dichroic mirrors, glass filters and detectors are plotted in Fig. 3. The *V* passband approximates that of Johnson's, while the *R* and *I* passbands approximate those of Cousins (Bessel 1979, 1993). The selection of the required glass filters are based on the filter-detector combinations used by Piirola (1973) and Hough et al. (1991); these authors also have employed dichroic filters to isolate spectral regions in their multiband polarimeters. The details of the filter-detector combinations used are given in Table 1.

The mean wavelength, calculated using

$$\lambda_0 = \frac{\int \lambda\, S(\lambda)\, \delta\lambda}{\int S(\lambda)\, \delta\lambda},$$

is also given in the table against the respective spectral band; $S(\lambda)$ is the wavelength-dependent responses plotted in Fig. 3.

The pulse amplifier-discriminators of Model ETL AD6 and Hamamatsu Model C9744 are used to interface the ETL 9893Q/350 and Hamamatsu R943-02 photomultiplier tubes, respectively, to the pulse counters. The uncooled ETL 9893Q/350 photomultiplier tubes used in the *U* and *B* bands give dark counts which are less than 10 counts s^{-1} at an ambient temperature of about 25°C when operated at an anode voltage of 2300 V. These are mounted in uncooled ambient ETL B2F-type housings, while the Hamamatsu tube used in the *VRI* channel is mounted in a FACT 50 model housing, which is of forced air-cooled type and cools about 50°C below an ambient temperature of 20°C. The dark counts given by the cooled tube when operated at a cathode voltage of –1900 V are also less than 10 counts s^{-1}.

A Glan-Taylor prism of 24.5 mm clear aperture, also acquired from Bernhard Halle Nachfl. GmbH, can be inserted in the telescope light path to produce a fully polarized beam that is necessary to measure and periodically check out the constancy of the polarization efficiency of the instrument. Facilities for wide angle-viewing and diaphragm-viewing have also been provided in the instrument for the easy acquisition of the object for observation.

4.   Control electronics

All the polarimeter functions are performed by two PIC family PIC16F877A1 microcontrollers. One microcontroller controls both the step motor coupled to the half wave plate and the servo motor coupled to the chopper wheel. The second microcontroller interfaces with the Linux machine, which is used to operate the polarimeter, through the standard serial communication with the RS232C protocol. The two microcontrollers in the instrument communicate between them through the built-in SPI Bus.

We have used a command-based communication protocol, wherein the computer acts as the master and the microcontroller as a slave unit. Always the commands are generated from the computer and sent to the microcontrollers, which interpret and execute them, and then respond indicating the status of the execution to the computer. We followed this scheme to avoid any communication clash between the computer and the microcontrollers, and to identify the errors, if any, quickly.

5.   Data acquisition and reduction procedure

5.1   Observations

The photomultiplier pulses corresponding to the intensities of the two emergent beams from the beam-displacement prism are counted separately over a full rotation of the halfwave plate at the specified equal angular intervals, starting from a reference position. The actual counting time interval for each beam over a rotational cycle of the chopper depends on its frequency of rotation since the latching pulses for the electronic pulse counters are derived from the positional sensors of the chopper. When the integrated counting time over several rotational cycles of the chopper equals to what is specified, the counting is stopped, and the resulting counts are stored. The halfwave plate is then moved to its next position, and the process is repeated at all the required positions. The entire procedure is counted as one cycle. The cycle can be repeated till the required accuracy in the measurement is achieved. After each cycle, the counts are added to the previously stored counts at the respective position of the halfwave plate. Before a new cycle begins the halfwave plate is always brought to its reference position. In order to give equal weightage to the observations in the data reduction, the number of counts accumulated at all positions of the half-wave plate should be of the same order. This requires that under poor sky conditions the observations should be repeated over several cycles of rotation of the half-wave plate, with a smaller integration time at each position of the halfwave plate. Usually, the observations in *U* and *B* bands will last longer than those in *V*, *R* and *I* bands. The integrations in *U* and *B* can be continued till integrations in the other bands are completed successively.

   The procedure is the same for the object and the sky background that has to removed from the object *plus* sky background counts before the data reduction. As shown in section 5.3 on optimum background sky observation, the time to be spent on sky integration is usually a small fraction of the time spent on the object integration. The optimum number of sky cycles for an observed number of object cycles and the optimum number of object cycles for an observed number of sky cycles, which are computed from the relative brightnesses of the object and sky, are displayed on the monitor.

   After each cycle, the linear polarization, the position angle and the gain-ratio, and their probable errors are displayed on the monitor. If the sky background is observed first, the displayed values will represent the actual values, otherwise they will only be approximations. Once the integration of the object is terminated, the final values of the Stokes parameters Q and U, the polarization (P%), the position angle ($\theta°$) and the mean Julian day of observation are stored in appropriate files.

5.2   Data reduction

The pair of counts registered at each position i of the halfwave plate depends both on the Stokes parameters I, Q and U of the incident light and the angle ψ^i between the optical axes of the two

halfwave plates at that position as given below:

$$N_1^i = \tfrac{1}{2} G_1 \, (I + Q \, \cos 4\psi^i + U \, \sin 4\psi^i) \, T_{atm} \quad \text{and}$$
$$N_2^i = \tfrac{1}{2} G_2 \, (I - Q \, \cos 4\psi^i - U \, \sin 4\psi^i) \, T_{atm} \, ,$$

where the subscripts 1 and 2 refer to the beams polarized in the principal plane of the first plate of the calcite block and the plane perpendicular to it, respectively. The parameters G_1 and G_2 are the net efficiencies for the two light beams, which include the transmittances and reflectivities of the various optical elements in the light path and the quantum efficiencies of the cathode of the photomultiplier tube, and T_{atm} is the atmospheric transmittance integrated over the period of observation. Taking the ratio of the counts accumulated in the two channels,

$$Z^i = \frac{N_1^i}{N_2^i} = \frac{1 + q \, \cos 4\psi^i + u \, \sin 4\psi^i}{\alpha \, (1 - q \, \cos 4\psi^i - u \, \sin 4\psi^i)} \, ,$$

where $\alpha \, (= G_2/G_1)$ is the ratio of the efficiencies of the two channels (gain-ratio), and q and u are the normalized Stokes parameters, (Q/I) and (U/I).

There will be M such ratios corresponding to the M positions of the halfwave plate over its full rotation at which the photons in the two beams are counted. The Stokes parameters and the gain-ratio are solved using the least-square method from these M ratios. The normal equations are solved using the Cracovian matrix elimination method (Kopal 1959) because it also gives the weights required to calculate the probable errors in the parameters that are solved for from the resulting standard deviation of the least square fit.

The percentage linear polarization P, position angle θ and their probable errors, ϵ_P and ϵ_θ, are calculated from

$$P\,(\%) = \sqrt{q^2 + u^2} \times 100 \, ,$$
$$2\,\theta = \tan^{-1}(u/q) \, ,$$
$$\epsilon_P\,(\%) = \frac{\sqrt{(q \, \epsilon_q)^2 + (u \, \epsilon_u)^2}}{p} \times 100 \quad \text{and}$$
$$\epsilon_\theta\,(\text{degree}) = \frac{28.65 \, \sqrt{(q \, \epsilon_u)^2 + (u \, \epsilon_q)^2}}{p^2} \, ,$$

where ϵ_q and ϵ_u are the probable errors in q and u, determined from the least square solution.

5.3   Optimum background sky observation

As already mentioned, the time to be spent on sky integration is usually a small fraction of the time spent on the object integration for the minimum error in the polarization determined, which arise from the statistical fluctuations in the photons counted. If n_1^i and n_2^i are the observed star

plus background sky counts at the ith position of the halfwave plate, and s_1 and s_2 are the scaled background sky counts due to the two beams,

$$N_1^i = n_1^i - s_1 \text{ and } N_2^i = n_2^i - s_2.$$

If we assume the gain-ratio to be unity, which is expected to be close to unity in normal cases, the conditions for least square give

$$q = \frac{\sum(Z_i^2 - 1)\,\cos 4\psi_i\,\sum(1 + Z_i)^2\,\sin^2 4\psi_i - \sum(Z_i^2 - 1)\,\sin 4\psi_i\,\sum(1 + Z_i)^2\,\sin 4\psi_i\,\cos 4\psi_i}{\sum(1 + Z_i)^2\,\cos^2 4\psi_i\,\sum(1 + Z_i)^2\,\sin^2 4\psi_i - (\sum(1 + Z_i)^2\,\sin 4\psi_i\,\cos 4\psi_i)^2}.$$

Further, if we assume that the observed polarization is small so that the squares and higher order terms in q and u can be neglected, and that the measurements are done over a full rotation of the halfwave plate at equal angular intervals, the expression for the differential in q can be written as

$$M\,n_*\,\delta q = \sum X_i\,(1 + Z_i)\,\delta n_1^i - \sum X_i\,(1 + Z_i)\,Z_i\,\delta n_2^i - \delta s_1 \sum X_i\,(1 + Z_i) + \\ \delta s_2 \sum X_i\,(1 + Z_i)\,Z_i\,, \quad (1)$$

where

$$X_i = Z_i\,\cos 4\psi_i - q\,(1 + Z_i)\,\cos^2 4\psi_i - u\,(1 + Z_i)\,\sin 4\psi_i\,\cos 4\psi_i$$

and n_* is the counts corresponding to the Stokes parameter I, the intensity due to the object alone.

The gain ratio of the beams α is usually close to unity and $q \ll 1$, making the counts n_1^i's and n_2^i's, and the statistical errors in their determination similar. Since photons obey Poisson statistics, we have $\sigma_n = \sqrt{n}$, in general. Assuming $\sigma_{n_1^i} = \sigma_{n_2^i} = \sigma_n$ and $\sigma_{s_1} = \sigma_{s_2} = \sigma_s$, using the law of propagation of errors, from Equation 1 we get

$$(\sigma_q)^2 = \frac{4}{M\,n_*^2}\left\{(\sigma_n)^2 + 2.5\,M\,q^2\,(\sigma_s)^2\right\}.$$

If $\bar{n}$ and $\bar{s}$, respectively, are the averages of the observed object *plus* background sky and background sky counts at various positions of the rotating half-wave plate in one second and if the object is observed for t_o and background for t_b seconds at each position of the half-wave plate, then

$$n_* = 2\,(n - s) = 2\,t_o\,(\bar{n} - \bar{s})\,,$$
$$(\sigma_n)^2 = t_o\,\bar{n} \quad \text{and} \quad (\sigma_s)^2 = (t_o/M\,t_b)^2\,M\,t_b\,\bar{s} = t_o^2\bar{s}/M\,t_b\,.$$

Making use of these values we get the probable error in q as

$$\epsilon_q = \frac{0.6745}{\sqrt{M}\,(\bar{n} - \bar{s})}\left(\frac{\bar{n}}{t_o} + 2.5\,q^2\,\frac{\bar{s}}{t_b}\right)^{\frac{1}{2}}.$$

There will be a similar relation for the other normalized Stokes parameter u. It is clear from the
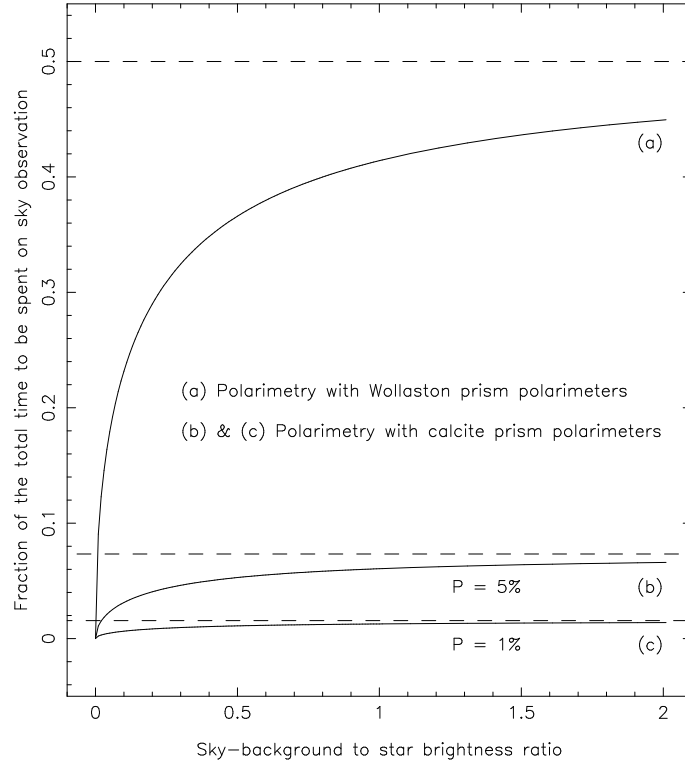
Figure 4. Plot of the optimum fraction of the time to be spent on background sky observation with the beam-displacement- and Wollaston prism-based polarimeters against the sky-background to star brightness ratio. The dashed lines show the corresponding asymptotic values.

above that the errors in q and u due to statistical fluctuations in the accumulated counts depend on the values of q and u themselves. When $\epsilon_q = \epsilon_u$, $\epsilon_p = \epsilon_q$. According to the above relation for the error due to photon noise $\epsilon_q = \epsilon_u$, when $q = u$, i.e., when $q = p/\sqrt{2}$. This implies that for a given linear polarization p, the observations would yield a minimum error in p if $q = u$, all other parameters being the same. The highest possible error in P due to photon fluctuations, which occurs when either $q = p$ and $u = 0$, or $u = p$ and $q = 0$, is obtained by replacing q by p in the above equation as

$$\epsilon_P(\%) = \frac{67.45}{\sqrt{M}\,(\bar{n} - \bar{s})} \left(\frac{\bar{n}}{t_o} + 2.5\,p^2\,\frac{\bar{s}}{t_b} \right)^{\frac{1}{2}} .$$

For an efficient use of the telescope time, we should distribute the total time available between the object and background sky observations such that the signal-to-noise ratio is a maximum, or equivalently, the error in P is a minimum. Differentiating the expression for $(\epsilon_P)^2$ with respect to t_o, the time spent on object integration, and equating it to zero, we get the condition for ϵ_P to be

a minimum as

$$\frac{t_b}{t_o} = p \sqrt{\frac{2.5 \, \bar{s}}{\bar{n}}} \, . \tag{2}$$

In polarimeters where the beam separation is large, the moon lit background sky will be modulated by the rotating half-wave plate because of its polarization. The intensities of the ordinary- and extraordinary-components at each position of the half-wave plate should be measured separately and removed from the object *plus* background data. When we deal with such a situation, s_1 and s_2 appearing in the above equations should be replaced by the corresponding s_1^i's and s_2^i's, which have uncorrelated statistical errors. The equation for $(\epsilon_P)^2$ then would be modified to

$$\epsilon_P(\%) = \frac{67.45}{\sqrt{M} \, (\bar{n} - \bar{s})} \left(\frac{\bar{n}}{t_o} + \frac{\bar{s}}{t_b} \right)^{\frac{1}{2}} ,$$

and the condition for ϵ_P to be a minimum as

$$\frac{t_b}{t_o} = \sqrt{\frac{\bar{s}}{\bar{n}}} \, .$$

Fig. 4 shows the fraction of the time to be spent on background sky observations as a function of the ratio of the background brightness to the object brightness with two different types of polarimeters, one with well separated ordinary- and extraordinary-beams as in the case of Wollaston or Foster prism-based polarimeters, and the other with overlapping ordinary- and extraordinary-beams as in the case of beam-displacement prism-based polarimeters. In the case of overlapping beam polarimeters the fraction of time to be spent on background observation increases with the polarization of the object and at low polarization levels, which is usually encountered in stellar polarization measurements, it is negligibly small, indicating that most of the available time can be spent on observing the object, and thereby, partially compensating for the loss in efficiency in not utilizing 50 per cent of the light collected by the telescope.

6.   Observational validation

The two main parameters of a polarimeter that determine its suitability for observations are the polarization it produces for an unpolarized beam and its ability to measure correctly the degree of polarization of a polarized beam without causing any depolarization; during February–April 2015 we observed unpolarized stars with and without the Glan-Taylor prism in the telescope beam to determine these two. Observations during April–May 2014 were made with different settings of the chopper speed, number of positions of the halfwave plate over a full rotation, integration times and diaphragm sizes, in order to look for any dependency on their values. Since we could not find any obvious differences in the results of those observations, all the observations made during February–April 2015, which are discussed here, were done with a chopper frequency of 50 Hz, 25 positions of the halfwave plate over a full rotation, integration time of 1-s, and diaphragms of 20 arc sec diameter. In addition to the *UBVRI* bands, another broad spectral band which included both the *R* and *I* bands was also used for the observations. We refer to this band, which has a mean wavelength of 712 nm, in this paper as *R′*.
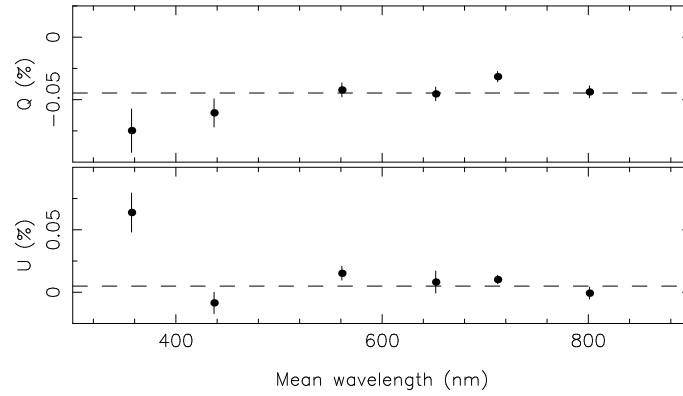
Figure 5. Plots of instrumental Q (%) and U (%) against the mean wavelength of the corresponding spectral band. The dashed lines show the averages of the corresponding quantities in the *BVRR′I* bands.
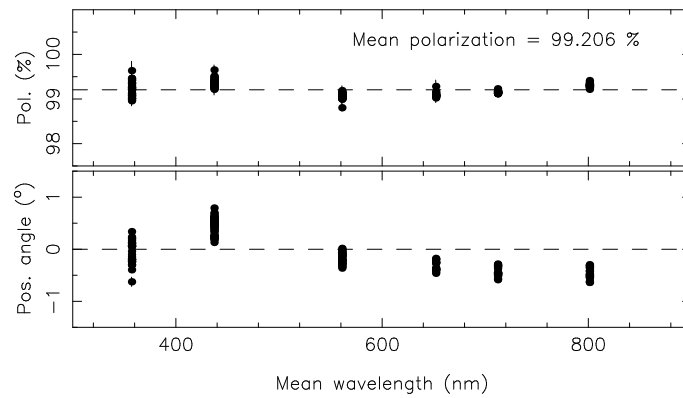

Figure 6. Plots of polarization efficiency and position angle against the mean wavelength of the corresponding spectral band. The dashed lines show the corresponding mean values.

6.1 Instrumental polarization

We observed the unpolarized stars, HD 42807, HD 65583, HD 90508, HD 98281, HD 103095, HD 100623, HD 125184 and HD 144287, on several occasions. The average values of the observed Q (%) and U (%) in the *UBVRR′I* bands are plotted against the mean wavelengths of the spectral bands in Fig. 5. It is clear that the polarization produced by the telescope-polarimeter combination, which is usually referred to as the instrumental polarization, is small. The instrumental polarization, apparently, increases slightly towards the ultraviolet. It is nearly constant in the $V - I$ spectral region.
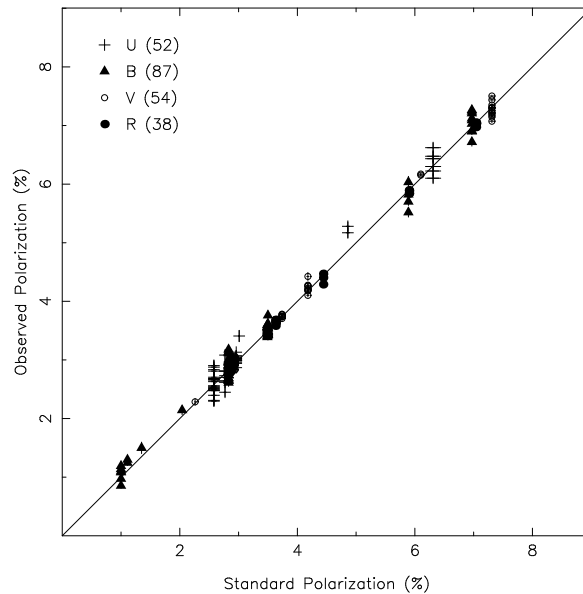
Figure 7. Plot of observed polarization against that available in the literature. The observed polarization has been corrected for the wavelength-dependent polarization efficiency and the instrumental polarization. The straight line indicates an efficiency of 100 per cent for the polarimeter. The number inside the brackets indicates the number of observations obtained in the corresponding spectral band.

6.2 Polarization efficiency

A total of 161 observations of several unpolarized stars were made with the Glan-Taylor prism in the light path of the telescope beam to determine the polarization efficiency of the instrument, which is the numerical value obtained by the instrument for an input beam that is 100% polarized. In the top panel of Fig. 6 we have plotted the individual values of the polarization efficiencies obtained by us in $UBVRR'I$ spectral bands against the corresponding mean wavelength. The polarization efficiency has a slight wavelength dependence, with lower values in the $V-R$ spectral region. The mean polarization efficiency is 99.206% and its total amplitude of variation in the $U-I$ spectral region is 0.271%. The position angle of polarization observed, which is plotted in the bottom panel of Fig. 6, also shows a slight wavelength dependence. The wavelength dependence observed is almost an inverted and scaled-down version of the variation of the position angle of the effective optical axis theoretically computed for a super-achromatic halfwave plate (Serkowski 1974b), indicating that the fixed super-achromatic halfwave plate in the beam does not fully compensate for the variation in the position angle of the effective optical axis of the rotating plate because of the slight, but unavoidable errors in their fabrication. The total amplitude of variation in the position angle is only 0.92° and the wavelength-dependent offset in the position angle can be incorporated in the data reduction procedure easily.
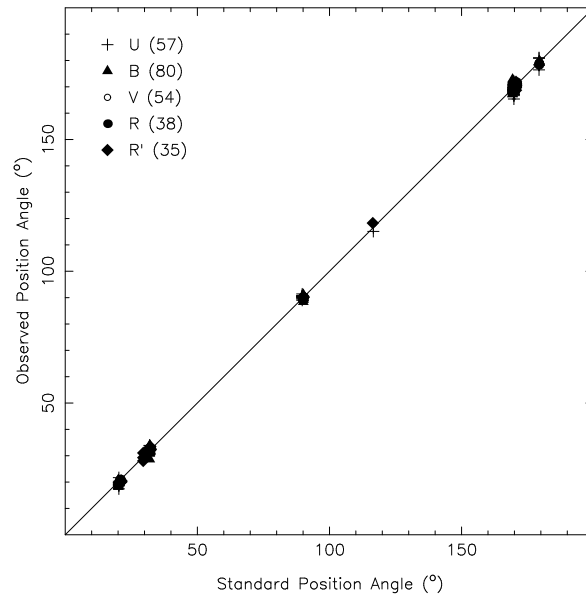
Figure 8. Plot of observed position angle against that available in the literature. The observed position angle has been corrected for the wavelength-dependent offset. The straight line has a slope of unity. The number inside the brackets indicates the number of observations obtained in the corresponding spectral band.

6.3   Observations of polarized stars

During the observing runs we observed the polarized stars, HD 21291, HD 23512, HD 43384, HD 147084, HD 154445, HD 160529, HD 183143, HD 58439, HD 94473, HD 127769 and HD 142863 in $UBVRR'I$ bands. Most of the above objects were observed several times during the observing runs. The first 7 objects are considered to be standard polarized stars, and are normally used to determine the offset in the measured position angles from the standard equatorial coordinate system. Hsu & Breger (1982) have reported polarizations and position angles for these objects in $UBVR$ bands. For the other 4 stars, Mathewson & Ford (1970) have given polarization measurements in the B spectral band. The above 4 stars were included in the present observations so as to have an extended range in the polarization and brightness for the observed polarized stars. In Fig. 7 we have plotted the polarization determined by us in $UBVR$ bands against the corresponding value available in the literature. The observed polarization has been corrected for the wavelength-dependent polarization efficiency of the instrument. It is clear from Fig. 7 that there is an excellent agreement between the measured polarization and the corresponding value available in the literature. A linear least square fit to the data plotted in the figure gives a value of 1.004±0.001 for the slope.

We have plotted in Fig. 8 the position angles observed by us in $UBVRR'$ against the corresponding values available in the literature. The position angles in R' band were obtained by an
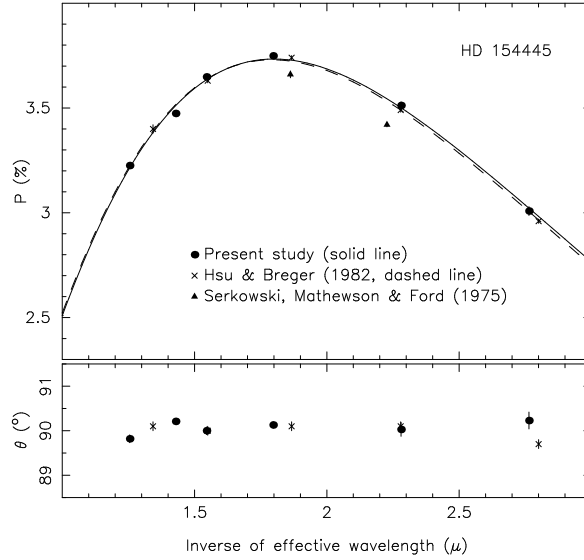
Figure 9. Plot of polarization in $UBVRR'I$ bands observed against the inverse of the corresponding effective wavelength. The solid ($P_{max} = 3.73 \pm 0.01$, $\lambda_{max} = 556 \pm 2$ nm) and dashed ($P_{max} = 3.73 \pm 0.01$, $\lambda_{max} = 558 \pm 2$ nm) lines show the computed interstellar polarization curves using the data obtained by us and Hsu & Breger (1982), respectively.

interpolation of the data given in Hsu & Breger (1982). It is clear that the agreement between the measured values and those available in the literature is very good. The observed position angles were corrected for the wavelength-dependent position angle of the effective optical axis of the rotating halfwave plate. The offset in the position angles was determined by a least square fit to the combined data plotted in Fig. 8. The offset obtained using such a procedure would be better than the value determined using a single standard polarized star, since, the position angles of some of the standards are found to vary by more than 1° (Hsu & Breger 1982).

In Fig. 9 we have plotted the averages of the polarization observed in $UBVRR'I$ bands against the corresponding inverse of the effective wavelength, which were computed using the responses of the filter-detector combinations, the $UBVRI$ magnitudes in the Johnson's system and the average extinction coefficients in those bands observed at Kavalur, for one of the polarization standards, namely, HD 154445. The airmass of observation was taken as 1.5. The figure also shows the observations of Hsu & Breger (1982) and Serkowski et al. (1975); the effective wavelengths of these observations were computed using the empirical relations given by the respective authors. The airmass of observation was taken as 1.0, while computing the effective wavelengths of the observations of Hsu & Breger (1982). The position angle of polarization of the object is plotted in the bottom panel of the figure.

We have also plotted in Fig. 9 the interstellar polarization curves, computed using the empirical relation given by Serkowski et al. (1975). The P_{max}, the maximum value of polarization,

and λ_{max}, the wavelength at which the maximum occurs, of the present data were derived using a least square fit of the empirical relation. Hsu & Breger (1982) have given P_{max} and λ_{max} for their data. It is clear from the figure that the present observations are in excellent agreement with those of Hsu & Breger (1982).

7. Conclusions

A new polarimeter for simultaneous observations in three spectral bands, *U*, *B* and *V*, or *R*, or *I* was designed and built in the Indian Institute of Astrophysics. A cross-mounted Calcite beam-displacement prism acts as the analyzer, and the modulation of the intensities of the emergent beams is achieved by a rotating superachromatic halfwave plate. Combinations of dichroic and Schott glass filters are used to isolate the spectral bands. In each spectral band the emergent beams from the analyzer are quasi-simultaneously detected by the same photomultiplier tube using a fast rotating chopper. The operation of the polarimeter is done using a Linux machine. All the functions of the polarimeter are controlled by the electronics built around PIC microcontrollers.

Since the background sky is not polarized when a beam displacement prism is used as the analyzer, time has to be spent only to determine the brightness of the background sky. We show from an analysis of the propagation of errors that the time to be spent on background observation is only a small fraction of the object integration for an optimum error in the observed polarization, which arise from the statistical fluctuations in the photon counts. This advantage partially offsets the loss in the efficiency of beam displacement prism-based polarimeters in not utilizing 50% of the light collected by the telescope.

The polarimeter was mounted onto the 1-m Carl Zeiss telescope at Vainu Bappu Observatory, and several unpolarized and polarized stars were observed during February–April 2015 to test its suitability for efficient astronomical observations. An analysis of the data collected showed the performance of the polarimeter to be quite satisfactory. The instrumental polarization, which includes the telescope contribution also, is found to be small. Observations with the Glan-Taylor prism in the light path show that both the polarization efficiency and the position angle of polarization are slightly wavelength-dependent; however, the total amplitudes of variation in the $U - I$ spectral region are only 0.271% and 0.92°. The mean polarization efficiency is found to be 99.206%. Both the polarization and position angles of standard polarized stars obtained using the polarimeter are in excellent agreement with those available in the literature.

Acknowledgments

References

Ashok N. M., Chandrasekhar T., Bhatt H. C., Manoj P., 1999, IAUC 7103

Bessel M. S., 1979, PASP, 91, 589

Bessel M. S., 1993, in Stellar Photometry − Current Techniques and Future Developments, IAU Coll. No. 136, Ed. C J. Butler, I. Elliott, Cambridge University Press

Deshpande M. R., Joshi U. C., Kulshrestha A. K., Bansidhar V. N. M., Majumdar H. S., Pradhan S. N., Shah C. R., 1985, BASI, 13, 157

Frecker J. E., Serkowski K., 1976, Appl. Optics, 15, 605

Hough, J. H., Peacock, T. & Bailey, J. A., 1991, MNRAS 248, 74

Hsu J., Breger M., 1982, ApJ, 262, 732

Jain S. K., Srinivasulu G., 1991, Opt. Eng., 30, 1415

Kameswara Rao N., Raveendran A. V., 1993, A&A, 274, 330

Kikuchi S., 1988, Bull. Tokyo Astron. Obs., Second Series No. 281, 3267

Kopal Z., 1959, Close Binaries, Chapman and Hall, London

Magalhaes A. M., Benedetti E., Roland E. H., 1984, PASP, 96, 383

Magalhaes A. M., Velloso, W. F., 1988, in Polarized Radiation of Circumstellar Origin, Eds: G.V. Coyne et al., Vatican Observatory, Vatican City State, p. 727

Manoj P., Maheswar G., Bhatt H. C., 2002, BASI, 30, 657

Mathewson D. S., Ford, V. L., 1970, Mem. Royal astr. Soc., 74, 139

Mekkaden M. V., 1999, A&A, 344, 111

Parthasarathy M., Jain S. K., Bhatt H. C., 2000, A&A, 355, 221

Piirola V., 1973, A&A, 27, 382

Raveendran A. V., 1999, MNRAS, 303, 595

Raveendran A. V., 2002, MNRAS, 336, 992

Raveendran A. V., Srinivasulu G., Muneer S., et al., 2015, A stellar photo-polarimeter, Technical Report, Indian Institute of Astrophysics, Bangalore 560034

Scaltriti F., Cellino A., Anderlucci E., Corcione L., Piirola V., 1989, MmSAI, 60, 243

Schwarz H. E., Piirola V., 1999, *Nordic Optical Telescope Operating Manual No. 2*

Serkowski K., 1974a, in Methods of Experimental Physics, 12 Part A, Eds M.L.Meeks, N.P.Carleton, Academic Press, New York, p. 361

Serkowski, K., 1974b, in Planets, Stars and Nebulae Studied with Photopolarimetry, Ed. T.Gehrels, Tucson, University of Arizona Press, p. 135

Serkowski K., Mathewson D. S., Ford V. L., 1975, ApJ, 196, 261

Young A. T., 1967, AJ, 72, 747